

# Learn the Force We Can: Multi-Object Video Generation from Pixel-Level Interactions

Aram Davtyan  
University of Bern  
Bern, Switzerland

aram.davtyan@unibe.ch

Paolo Favaro  
University of Bern  
Bern, Switzerland

paolo.favaro@unibe.ch

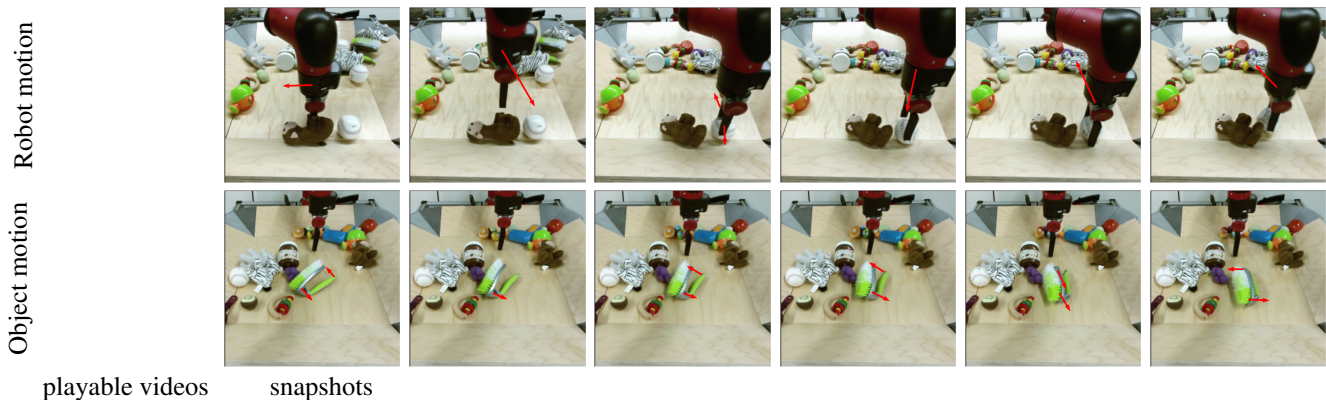


Figure 1: Examples of videos generated through controlled motions by YODA on the BAIR dataset. All videos are generated autoregressively by starting from a single image and then by providing control inputs in the form of 2D shifts (shown as red arrows superimposed to the frames). To play the videos in the first column on the left, view the paper with Acrobat Reader.

## Abstract

We propose a novel unsupervised method to autoregressively generate videos from a single frame and a sparse motion input. Our trained model can generate realistic object-to-object interactions and separate the dynamics and the extents of multiple objects despite only observing them under correlated motion activities. Key components in our method are the randomized conditioning scheme, the encoding of the input motion control, and the randomized and sparse sampling to break correlations. Our model, which we call YODA, has the ability to move objects without physically touching them. We show both qualitatively and quantitatively that YODA accurately follows the user control, while yielding a video quality that is on par with or better than state of the art video generation prior work on several datasets. For videos, visit our project website <https://araachie.github.io/yoda>.

## 1. Introduction

According to Judea Pearl and Dana Mackenzie [48], “a causal learner must master at least three distinct levels

of cognitive ability: seeing, doing and imagining.” The achievement of these levels seems to correlate well with the development of skills in organisms and with their chances of survival. For instance, organisms that learned how to use a tool (an example of *doing*), have better means to defend themselves beyond their genetic endowments, to capture preys and to build other useful structures, such as shelters. Among these levels, *imagining* is considered the most powerful capability. *Imagining* is the ability to ask and answer counterfactual questions such as “What would happen if X had moved differently than how it did in the past?”

In this work, we aim at building models that can learn how to answer such counterfactual questions through the generation of video in a completely unsupervised fashion. Learning is allowed only through the passive observation of videos, *i.e.*, without the ability to explicitly interact with the scene, and without any per-sample manual annotation. We do not aim to learn causal relationships [48, 69], but rather we aim more conservatively to build a model that can show some degree of generalization from the training data, *i.e.*, that can generate data that was not observed before, that is directly related to our question, and that is plausible,

as shown in Figure 1. We focus on counterfactual questions that can be formulated in the form of a motion specification, *i.e.*, “What would happen if the object containing this pixel would move at this location?” The questions are posed by providing the current frame, *context* frames (a subset of the past frames), and a motion control, *i.e.*, a shift at a pixel (but the model can also take multiple shifts at once and also at different time instants). The answer is a generated subsequent frame that shows how the input frame would change under the specified motion. We train our model **without** specifying what objects are (*i.e.*, we do not use information about object categories), or where they are (*i.e.*, we do not rely on bounding boxes, landmarks/point annotations or segmentation masks), or how they interact (*i.e.*, we do not make use of information on object relationships or action categories or textural descriptions of the scenes). Given two subsequent frames (the current and following one) from a video in our training data, we obtain the motion control input by sampling the estimated optical flow at a few (typically 5) locations. To generate frames we use flow matching [38, 40, 1], where the model is conditioned on the current and past frames [11], and feed the motion control input through cross-attention layers in a transformer architecture. We call our approach YODA, as it shows the ability of moving objects without touching them.

As shown in Figure 1, an emerging property of our proposed approach is that the model learns the physical extent of objects in the scene without ever requiring explicit supervision for it. For example, although the control is applied to the handle of the brush in the second row, the motion is applied correctly to the whole brush, and to the whole brush only. A second learned property can be observed on the first row: When the robot arm is driven towards other objects, it interacts with them realistically. In the second row, we can observe a third remarkable capability that the model has learned. The generated video shows that we can directly rotate a single object, without using the robot arm to do so. This is a video that has never been observed in the dataset (all objects are moved directly by the arm or indirectly via other objects). It does demonstrate empirically that the model has the ability to *imagine* novel plausible outcomes when the reality is modified in ways that were not observed before. Our contributions can be summarized as follows

1. We introduce a model for controllable video synthesis that is trained in a completely unsupervised fashion, is not domain-specific, and can scale up to large datasets;
2. We introduce an effective way to embed motion information and to feed it to the model, and show analysis to understand the impact of sampling and the use of sparsity of the motion field;
3. We demonstrate for the first time multi-object interac-

tions in the unsupervised setting on real data, which has not been shown in other state of the art methods [44, 43, 10, 29, 6, 5].

## 2. Prior Work

**Video generation.** An increased interest in video generation has followed the success of generative models for images [32, 15, 13, 50]. In contrast to image generation, video generation is plagued by problems such as rendering realistic motion, capturing diversity (*i.e.*, modeling the stochasticity of the future outcomes) and, most importantly, managing the high computational and storage requirements. Conventional approaches to video generation are autoregressive RNN-based models [3, 6]. RNNs are expected to generate sequences with a consistent motion, because of the conditioning on the previously generated frames. Other models instead obtain consistency through the direct generation of a predefined number of frames [24, 5, 54]. Variability (stochasticity) of the generated sequences has been tackled with GANs [9, 42, 36], variational approaches [2, 12, 3, 63, 37], Transformers [35, 49, 17, 53, 66] and diffusion-based approaches [24, 59, 26, 19, 21, 67]. The recently proposed autoregressive method RIVER [11] deals with the stochastic nature of the generative process through flow matching [38]. Among all above approaches, YODA uses RIVER as a backbone, because of its efficiency and ease of training.

**Controllable video generation** work mostly differs in the nature of the control signals. Control can be defined per frame [8, 16, 33, 45, 46, 27, 44, 10, 29, 51], or as a global label [34, 60, 54]. Some of them are obtained via supervision [8, 16, 33, 45, 46], or discovered in an unsupervised manner [44, 10, 29, 51]. For instance, CADDY [44] learns a discrete action code of the agent that moves in the videos. Another model, GLASS [10] decouples the actions into global and local ones, where global actions, as in YODA, are represented with 2D shifts, while local actions are discrete action codes, as in [44]. In [29] the authors explicitly separate the foreground agent from the background and condition the generation on the transformations of the segmentation mask. However, all these models are restricted to single agent videos, while YODA successfully models multiple objects and their interactions. [27, 18, 6, 5] are the most similar works to ours as they specify motion control at the pixel-level. However, [27] leverages a pre-trained object detector to obtain the ground truth control. [18] is based on warping and therefore does not incorporate memory to model long-range consequences of actions. II2V [6] uses a hierarchical RNN to allow modeling higher-order details, but focuses on deterministic prediction. iPOKE [5] aims to model stochasticity via a conditional invertible neural network, but has to sacrifice the ability to generate long videos and to intervene into the generation process at any timestamp. None of those works has demonstrated controllable



video generation on multi-object real scenes.

**Multi-object scenes and interactions.** Modeling multiple objects in videos and especially their interactions is an extremely difficult task. It either requires expensive human annotations [28] or is still limited to simple synthetic scenes [64, 52, 31]. [43, 65] allow for multi-agent control, but leverage ground truth bounding boxes during the training. YODA in turn is an autoregressive generative model for controllable video generation from sparse motion controls that i) efficiently takes memory into account to simulate long-range outcomes of the actions, ii) models stochasticity of the future, iii) does not require human annotation for obtaining the control signal(s), and iv) demonstrates controllability on a complex multi-object real dataset.

### 3. Training YODA

We denote with  $\mathbf{x} = \{x^1, \dots, x^N\}$  an RGB video that contains  $N$  frames, where  $x^i \in \mathbb{R}^{3 \times H \times W}$ ,  $i = 1, \dots, N$ , and  $H$  and  $W$  are the height and the width of the frames respectively. The goal is to build a controllable video prediction method that allows us to manipulate separate objects in the scene. We formulate this goal as that of approximating a sampler from the following conditional distribution

$$p(x^{k+1} | x^k, x^{k-1}, \dots, x^1, a^k), \quad (1)$$

for  $k < N$  and where  $a^k$  denotes the motion control input.  $a^k$  specifies the desired shifts at a set of pixels (including the special cases with a single pixel or none). Our ultimate objective is to ensure through training that this control implicitly defines the shift(s) for the object(s) containing the selected pixel(s). The conditioning in eq. (1) allows an autoregressive generative process at inference time, where the next frame  $x^{k+1}$  in a generated video is sampled conditioned on the current frame  $x^k$ , the previously generated frames  $x^{k-1}, \dots, x^1$  and the current control  $a^k$ . To model the conditional distribution in eq. (1), we use RIVER [11]. This is a recently proposed video prediction method based on conditional flow matching [38]. We chose RIVER due to its simplicity and training efficiency compared to conventional RNNs [3, 25, 2, 12, 36] and Transformers [58, 62, 35, 49, 17, 53] for video prediction. For completeness, we briefly introduce Flow matching and RIVER in section 3.1. In section 3.2 we show how the latter is adapted to handle control. In section 3.3, we focus on how the control signals are obtained and encoded.

#### 3.1. Preliminaries: Flow Matching and RIVER

**Flow matching** [38, 40, 1] was introduced as a simpler, more general and more efficient alternative to diffusion models [22]. The goal is to build an approximate sampler from the unknown data distribution  $q(y)$ , given a training set of samples of  $y$ . This is formalized as a continuous

normalizing flow [7] via the following ordinary differential equation

$$\begin{aligned} \dot{\phi}_t(y) &= v_t(\phi_t(y)) \\ \phi_0(y) &= y. \end{aligned} \quad (2)$$

Eq. (2) defines a flow  $\phi_t(y) : [0, 1] \times \mathbb{R}^d \rightarrow \mathbb{R}^d$  that pushes  $p_0(y) = \mathcal{N}(y | 0, 1)$  towards the distribution  $p_1(y) \approx q(y)$  along the vector field  $v_t(y) : [0, 1] \times \mathbb{R}^d \rightarrow \mathbb{R}^d$ . Remarkably, [38] shows that one can obtain  $v_t(y)$  by solving

$$\min_{v_t} \mathbb{E}_{t, p_t(y | y_1), q(y_1)} \mathcal{L}(\theta), \quad (3)$$

$$\text{with } \mathcal{L}(\theta) = \|v_t(y) - u_t(y | y_1)\|^2, \quad (4)$$

where one can explicitly define the vector field  $u_t(y | y_1)$  and its corresponding probability density path  $p_t(y | y_1)$ , with  $y_1 \sim q(y)$ . A particularly simple choice [38] is the Gaussian probability path  $p_t(y | y_1) = \mathcal{N}(y | \mu_t(y_1), \sigma_t^2(y_1))$ , with  $\mu_0(y_1) = 0, \mu_1(y_1) = y_1, \sigma_0(y_1) = 1, \sigma_1(y_1) = \sigma_{\min}$ . The corresponding target vector field is then given by

$$u_t(y | y_1) = \frac{y_1 - (1 - \sigma_{\min})y}{1 - (1 - \sigma_{\min})t}. \quad (5)$$

Sampling from the learned model can be obtained by first sampling  $y_0 \sim \mathcal{N}(y | 0, 1)$  and then by numerically solving eq. (2) to obtain  $y_1 = \phi_1(y_0)$ .

**RIVER** [11] is an extension of the above procedure to the video prediction task with a computationally efficient conditioning scheme on past frames. The training objective of RIVER is given by

$$\mathcal{L}_R(\theta) = \|v_t(x | x^{\tau-1}, x^c, \tau - c; \theta) - u_t(x | x^\tau)\|^2, \quad (6)$$

where  $v_t$  is a network with parameters  $\theta$ ,  $x^\tau$  is a frame randomly sampled from the training video,  $c$  is an index randomly sampled uniformly in the range  $\{1, \dots, \tau - 2\}$  and  $u_t$  is calculated with eq. (5). An additional information provided to  $v_t$  is the time interval  $\tau - c$  between the target frame  $x^\tau$  and the past frame  $x^c$ , which we call the *context frame*.

At test time, during the integration of eq. (2), a new context frame  $x^c$  is sampled at each step  $t$ . This procedure enables to condition the generation of the next frame on the whole past. To further speed up the training and enable high-resolution video synthesis, RIVER works in the latent space of a pretrained VQGAN [15]. That is, instead of  $x^\tau, x^{\tau-1}, x^c$  in eq. (6) one should write  $z^\tau, z^{\tau-1}, z^c$ , where  $z^i$  is the VQ latent code of the  $i$ -th frame [11]. Since the use of VQGAN encoding is an optional and separate procedure, we simply use  $x$  in our notation.

#### 3.2. Learning to Master the Force

We now show how to incorporate control into eq. (6) to build a sampler for the conditioning probability in eq. (1).

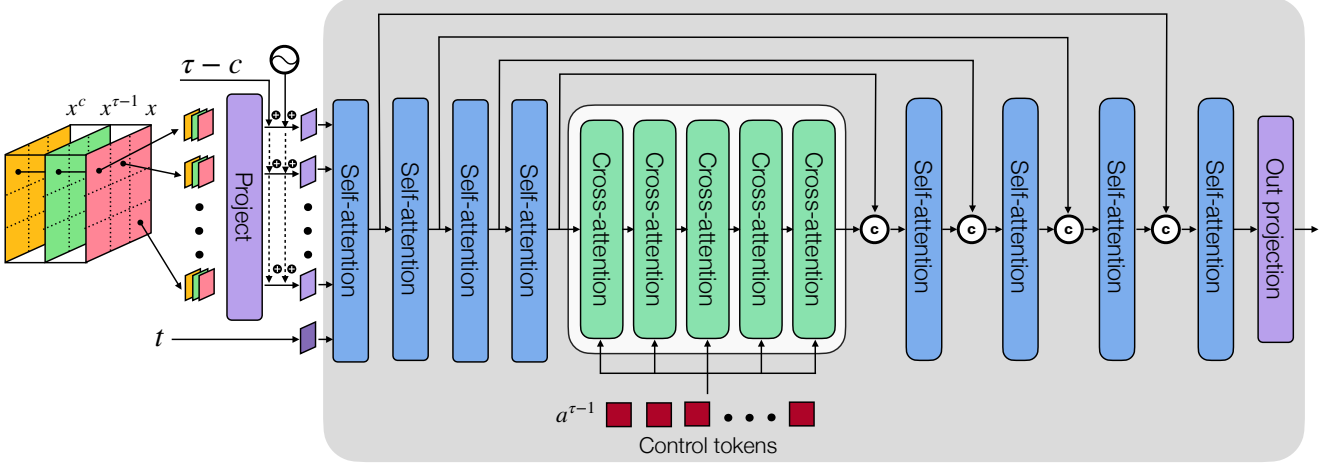


Figure 2: Overview of YODA’s architecture. The noisy target frame  $x$ , the reference frame  $x^{\tau-1}$  and the context frame  $x^c$  are concatenated, reshaped and projected to form a sequence of visual tokens that is augmented with position encodings and embedded relative temporal distance  $(\tau - c)$  between frames and fed to the U-ViT [4] alongside with the embedded time token  $(t)$ . A sequence of control tokens is fused into the pipeline via cross-attention in the bottleneck of the network.

To do so, we make  $v_t$  depend on  $a^{\tau-1}$ , which is the motion control at time  $\tau - 1$ , as shown in the following objective

$$\mathcal{L}_F(\theta) = \|v_t(x | x^{\tau-1}, x^c, \tau - c, a^{\tau-1}; \theta) - u_t(x | x^\tau)\|^2. \quad (7)$$

In practice, we implement this conditioning by substituting the bottleneck in the self-attention layers of the U-ViT [4] architecture of RIVER with cross-attention blocks (see Figure 2). The control inputs  $a^{\tau-1}$  are obtained by splitting the image domain into a grid of tiles, so that a motion control can be specified in each tile via a code, and then be fed as keys and values to the cross-attention layer. More details on  $a^{\tau-1}$  will be provided in the next section.

Inspired by the classifier-free guidance for diffusion models [23], we propose to switch off the conditioning on both the context and motion control at every iteration, with some probability  $\pi$  (see Algorithm 1). This is done by substituting the code corresponding to a switched off context or motion control with noise. A typical value for  $\pi$  in our experiments is 0.5. This serves two purposes: 1) it yields a stronger model that can effectively take the conditioning into account and 2) it yields a model that can generate a video by starting from a single frame. To see 1), consider that the conditioning on both the context frame  $x^c$  and the control  $a^{\tau-1}$  is redundant when the future frame can be reliably predicted given only one of the two. In these cases, the model might learn to ignore one of the inputs. To see 2), consider that when the model generates the first predicted frame, there is no valid context frame and our procedure allows us to replace the context frame with noise. Otherwise, one would have to duplicate the first frame, for example, but this would result in an undesirable training bias.

#### Algorithm 1 Training of YODA

- 1: Input: dataset of videos  $D$ , number of iterations  $N$ ;
- 2: **for**  $i$  in range( $1, N$ ) **do**
- 3:   Sample a video from the dataset  $\mathbf{x} \sim D$  of length  $L$ ;
- 4:   Choose a random target frame  $x^\tau, \tau \in \{3, \dots, L\}$
- 5:   Sample a timestamp  $t \sim U[0, 1]$ ;
- 6:   Sample a noisy observation  $x \sim p_t(x | x^\tau)$ ;
- 7:   Calculate  $u_t(x | x^\tau)$  according to eq. (5);
- 8:   Sample a condition frame  $x^c, c \in \{1, \dots, \tau - 2\}$ ;
- 9:   Compute the control  $a^{\tau-1}$  (see sec. 3.3);
- 10:   With probability  $\pi$  set  $x^c$  to noise;
- 11:   With probability  $\pi$  set  $a^{\tau-1}$  to noise;
- 12:   Take a gradient descent update  $\theta \leftarrow \theta - \alpha \nabla_\theta \mathcal{L}_F(\theta)$  with learning rate  $\alpha > 0$ ;
- 13: **end for**

### 3.3. Force Embeddings

Ideally,  $a^{\tau-1}$  could encode detailed motion information for the objects in the scene. For instance,  $a^{\tau-1}$  could describe that an object is rotating or pressing against another object or walking (in the case of a person). Such supervision could potentially provide the ability to control the video generation in detail and to generalize well to unseen object motion combinations. However, obtaining such ground truth control signals requires costly large-scale manual annotation. Similarly to [5], we avoid such costs by leveraging optical flow. Essentially, instead of using a costly and detailed motion representation, we use a simpler one that can be computed automatically and at a large scale.

Given an optical flow  $w^\tau \in \mathbb{R}^{2 \times H \times W}$  between

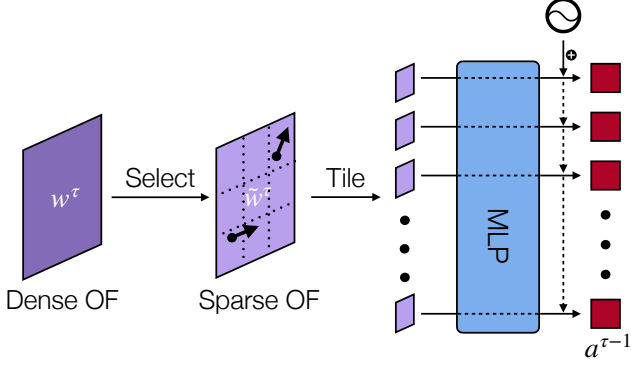


Figure 3: Sparse optical flow (OF) encoder. The dense OF is sampled and tiled in a  $16 \times 16$  grid. Each OF tile is fed independently to the MLP, and then combined with a learnable positional encoding into a code.

the frames  $x^\tau$  and  $x^{\tau+1}$  (obtained with a pretrained RAFT [55]), we define a probability density function  $p(i, j) \propto \|w_{ij}^\tau\|^2$  over the image domain  $\Omega$ , with  $(i, j) \in \Omega$ . Then, we randomly sample a sparse set  $\mathcal{S} \subset \Omega$  of  $n_c = |\mathcal{S}|$  pixel locations from  $p$ . This distribution makes it more likely that pixels of moving objects will be selected. However, in contrast to [5] we do not introduce additional restrictions to the sampling or explicitly define the background. This is an essential difference, because in multi-object scenes, objects that belong to the background in one video might be moving in another. Thus, in our case, one cannot use the magnitude of the optical flow to separate objects from the background in each video.

To condition the video generation on the selected optical flow vectors, we introduce an encoding procedure. First, we construct a binary mask  $m \in \{0, 1\}^{1 \times H \times W}$  such that  $m_{ij} = 1, \forall (i, j) \in \mathcal{S}$  and  $m_{ij} = 0$  otherwise. This mask is concatenated in the channel dimension with  $m \odot w^\tau$  to form a tensor  $\tilde{w}^\tau$  of shape  $(3, H, W)$ , which we refer to as the *sparse optical flow*.  $\tilde{w}^\tau$  is further tiled into a  $16 \times 16$  grid. Each of these tiles is independently projected through an MLP and augmented with a learnable positional encoding to output a code (see Figure 3). This particular design of the optical flow encoder is a trade-off between having a restricted receptive field (because each tile is processed independently) and efficiency. A small receptive field is needed to ensure that separate controls minimally interact before being fed to the cross-attention layers (see Figure 2). We found that this is crucial to enable the independent manipulation of separate objects.

## 4. Experiments

In this section, we evaluate YODA to see how controllable the video generation is, *i.e.*, how much the generated

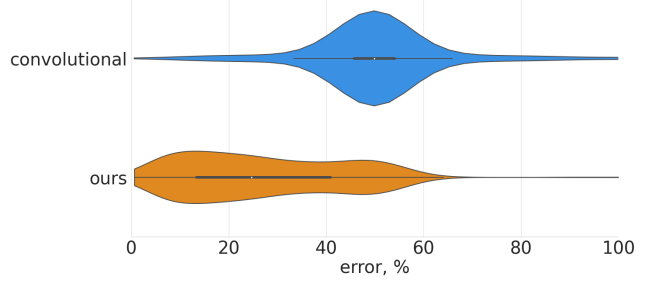


Figure 4: Violin plots of the control vs generated motion error distributions. On the top is the distribution of the errors obtained when using a convolutional encoding of the motion controls (*i.e.*, with a large receptive field). At the bottom is the distribution obtained with the chosen encoding (*i.e.*, with a limited receptive field). The chosen encoding decreases the average error and also makes the model more stable (there is no long tail).

object motion correlates with the input motion control (see next section), and to assess the image and sequence quality on three datasets with different scene and texture complexities, as well as different object dynamics. In the latter case, we report several video quality metrics, such as FVD [57] and average LPIPS [70], PSNR, SSIM [61] and FID [47]. Implementation and training details are provided in the supplementary material.

### 4.1. Evaluation of Intended vs Generated Motion

The objective of our training is to build a model to generate videos that can be controlled by specifying motion through  $a^{\tau-1}$  as a set of shifts at some user-chosen pixels. To evaluate how much the trained model follows the intended control, we introduce the following metrics: Local and global errors. To compute them, we sample an image from the test videos. Then, we randomly select one object in the scene and apply a random motion control input to a pixel of that object. Because the generated images are of high-quality, we can use a pre-trained optical flow estimation model [55] to calculate the optical flow between the first image and the generated one. In principle, one could measure the discrepancy between the input motion shift and the generated one at the same pixel. However, since single pixel measurements are too noisy to use, we assume that all pixels within a small neighborhood around the selected pixel move in the same way, and then average the estimated optical flow within that neighborhood to compare it to the input control vector (depending on what we focus on, we use the relative  $L_2$  norm or a cosine similarity). We call this metric the *local error* (see Figure 5 on the left in blue). Notice that in some cases, the model could use the motion input to generate a rotated object, instead of a translated one. Also, the chosen neighborhood (whose size is fixed)



may not fully cover only the object of interest. These issues make this metric quite noisy. Nonetheless, it still provides a useful approximation of the average response of the trained model to the control inputs. We also assume that the generated motion should be zero sufficiently far away from where the motion control is applied, although in general a local motion could cause another motion far away. To assess this, we calculate the average  $L_2$  norm of the estimated optical flow outside some neighborhood of the controlled pixel. We call this metric the *global error* (see Figure 5 on the right in orange). This measurement tells us the spatial extent of the learned motion control correlations.

## 4.2. Datasets

We evaluate YODA on the following three datasets:

**CLEVRER** [68] is a dataset containing 10K training and 1000 test videos capturing a synthetic scene with multiple simple objects interacting with each other through collisions. We cropped and downsampled the videos to  $128 \times 128$  resolution. On CLEVRER we show the ability of our model to model complex cascading interactions and also to learn the control of long-term motions (*i.e.*, motions that once started at one frame can last for several frames).

**BAIR** [14] is a real dataset containing around 44K videos of a robot arm pushing toys on a flat square table. The resolution of these videos is  $256 \times 256$  pixels. The visual complexity of BAIR is much higher than that of CLEVRER. The objects on the table are diverse and include non-rigid objects, such as stuffed toys, that have different physical properties. However, in contrast to CLEVRER, its interactions are simpler and do not require modeling long-term dynamics.

**iPER** [39] captures 30 humans with diverse styles performing various movements of varying complexity. The official train/test split separates the dataset into 164 training and 42 test clips. Although our main focus is to work with multi-object datasets, we use this dataset for two reasons: 1) We can test how YODA learns to control articulated objects, such as humans; 2) We can compare to the related work iPOKE [5], which has already been tested on this dataset (and is not designed for multi-object datasets).

## 4.3. Ablations

**Sparse optical flow encoder.** First, we show the importance of using a sparse optical flow encoder with a restricted receptive field. We observe that such an encoder is essential for the model to learn to independently control different objects in the scene. We manually annotated 128 images from the test set of the BAIR dataset. For each image we store a list of pixel coordinates that belong to objects in the scene, 1-2 pixels per object, 3 pixels for the robot arm. We use the local error to compare our encoder with a convolutional sparse optical flow encoder from [5]. In Figure 4, we

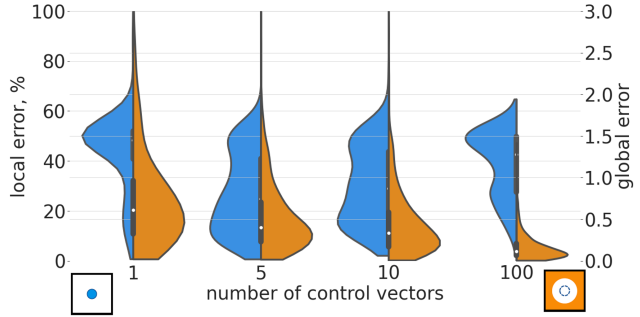


Figure 5: The effect of number of control vectors used during the training. The *local error* (in blue and on the top) stands for the error of the optical flow in the neighborhood of the controlled pixel, while the *global error* (in orange and at the bottom) is the average optical flow vector outside of a circle around the interacted pixel. A smaller local error indicates a better response of the model to the control, while a low global error ensures that only the object of interest moves. The boxes at the bottom illustrate the regions across which the error is averaged (left - local error, right - global error). Best viewed in color.

$n_c$	$\pi$	LPIPS↓	PSNR↑	SSIM↑	FID↓	FVD↓
5	0.5	0.126	30.07	0.93	5.7	70
1	0.5	0.144	28.78	0.92	6.3	83
5	0.0	0.288	24.88	0.86	9.9	401

Table 1: Evaluation of the generated videos on CLEVRER under different input sparsity ( $n_c$ ) and randomization ( $\pi$ ).

show that our restricted receptive field optical flow encoder outperforms the convolutional one.

**Randomized conditioning.** In Table 1, we demonstrate the importance of our randomized conditioning scheme, where we randomly switch off the conditioning with respect to both the past frame and the control input with probability  $\pi$ . The comparisons on the CLEVRER dataset show that randomized conditioning is crucial for the single frame quality as well as for temporal consistency (see the FVD metric).

**Number of control inputs during the training.**  $n_c$  plays an important role in enabling the independent control over separate objects. In principle, responses to the control should be more and more decorrelated as we increase the number of control inputs. However, values of  $n_c$  that are too large would increase the gap between the training and the test conditions, where often only 1 control is used. At the same time, using fewer optical flow vectors during the training stimulates the network to learn interactions (*i.e.*, correlations with other objects). Therefore, we observe a trade-off between controllability and learning correct dynamics in the choice of  $n_c$  (see Figure 5). We choose  $n_c = 5$  in the remaining experiments.

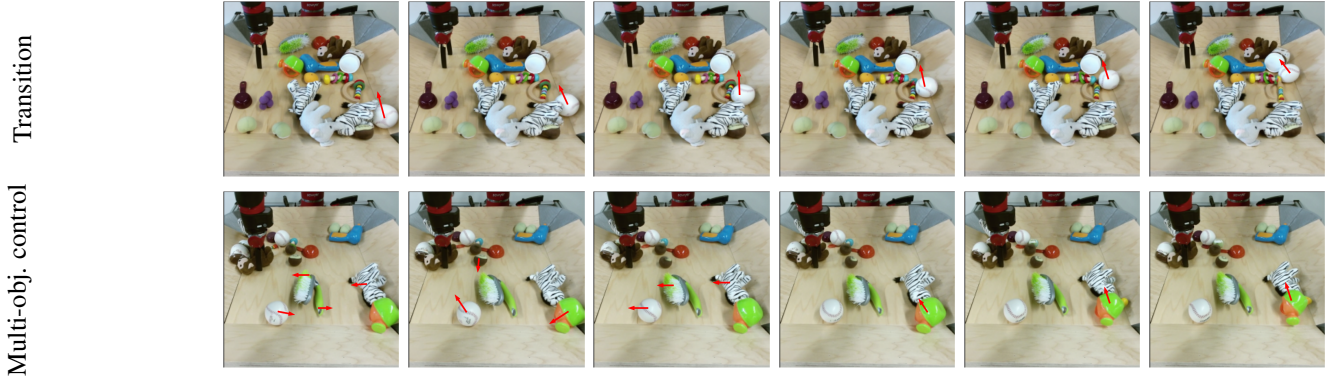


Figure 6: More object manipulation scenarios with YODA on the BAIR dataset. The vectors in red are the control signals specified per frame in an interactive regime. The images in the first column can be played as videos in Acrobat Reader.

Method	LPIPS↓	FID↓	FVD↓
MoCoGAN [56]	0.466	198.0	1380
MoCoGAN+ [44]	0.201	66.1	849
SAVP [36]	0.433	220.0	1720
SAVP+ [44]	0.154	27.2	303
CADDY [44]	0.202	35.9	423
Huang et al. [29] <i>positional</i>	0.202	28.5	333
Huang et al. [29] <i>affine</i>	0.201	30.1	292
Huang et al. [29] <i>non-param</i>	0.176	29.3	293
GLASS [10]	0.118	18.7	411
YODA (ours) <i>5 controls</i>	<b>0.112</b>	<b>18.2</b>	<b>264</b>
YODA (ours) <i>1 control</i>	0.142	19.2	339

Table 2: Video quality comparisons on the BAIR dataset.

#### 4.4. Quantitative results

**Realism and motion consistency.** Following [44], we train YODA on BAIR and then autoregressively generate 29 frames given the first frame and a set of controls at each generation step, decoded from the ground truth videos (in our case from the corresponding optical flows). We report the metrics for 1 and 5 control vectors at each timestamp and show that the *5 controls* version outperforms all prior work (see Table 2). Moreover, notice that prior work on controllable generation on BAIR only focuses on modeling the actions of the robot arm, while YODA is able to also effectively control other objects in the scene. We also compare our model on the benchmark introduced in [5] and generate 9 frames starting from a single initial frame. Although our model does not outperform [5], it does better than all the other prior work, as indicated by our FVD metric (see Table 3). One should also notice that YODA does not make use of the same information used in iPOKE [5] (e.g., what a background is).

**Scene dynamics and interactions.** We chose to assess how well YODA models the physics of the scene and object interactions on the CLEVRER dataset. For this purpose, we generate 15 frames starting from a single frame and a set of

Method	FVD↓	LPIPS↓	SSIM↑
Hao [18]	235.08	0.11	0.88
Hao [5] w/ <i>KP</i>	141.07	<b>0.04</b>	<b>0.93</b>
II2V [6]	220.34	0.07	0.89
iPOKE [5]	<b>77.50</b>	0.06	0.87
YODA (ours) <i>1st frame</i>	133.08	0.09	0.86
YODA (ours) <i>all frames</i>	134.35	0.09	0.87

Table 3: Video quality comparisons on the iPER dataset.

control vectors. This time we do not specify future controls like in BAIR and let the model simulate the learned physics. We repeat the experiment with 1 and 5 control vectors. The metrics in Table 1 show that YODA models the interior object dynamics well, which is further supported by the qualitative results in section 4.5.

**Controllability.** We assess how robust YODA is to changes in the control parameters, such as the direction and the magnitude of the control vectors. We manually annotated 128 images from the CLEVRER dataset by indicating 1 potential control point per object. We then sample some points and random control vectors from the annotated ones and feed those to the model to generate the next frame. We calculate the error between the control vectors and the average computed optical flow [55] in the neighborhood of the interacted pixel. We use the cosine distance between the normalized vectors as an indicator of the accuracy of the control. We show how this metric changes with the parameters of the control in Figure 7.

#### 4.5. Qualitative results

In this section we provide some visual examples of the generated sequence. On the BAIR dataset, we highlight the capability of YODA to move, rotate and deform separate objects without the robot arm physically touching them. Figures 1 and 6 show different object manipulations on the BAIR test set. Notice how the model has learned also the

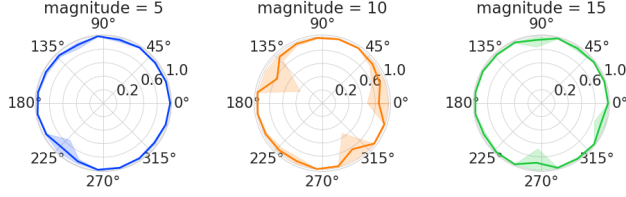


Figure 7: Average cosine error between the control vector and the resulting optical flow depending on the magnitude of the control (in pixels) and its direction on CLEVRER.

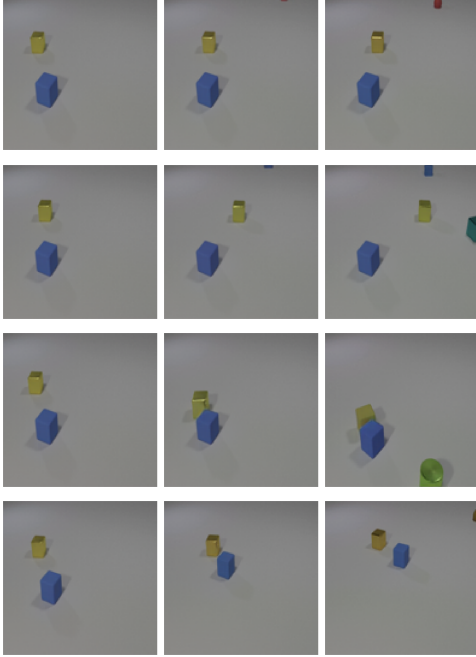


Figure 8: The leftmost frame is the same across all four rows. In each row YODA is given the controls indicated as a red arrow on the leftmost column. YODA follows accurately the magnitude (first to second rows) and direction (first to third rows) of the motion control input, as well as multiple inputs (fourth row). Notice that since YODA has memory and was trained also to generate frames without control, it can learn to propagate motion across many frames from a single initial control input. The images in the first column can be played as videos in Acrobat Reader.

3D representations and interactions of the objects. Figure 8 shows the diversity of generated videos that share the same initial frame, but use different control signals. Notice the high correlation between the intended and generated motions and the ability of the model to correctly predict the interactions between the colliding objects. Since our model is based on Transformers [58], we report the attention maps from the last layer of the network between the interacted

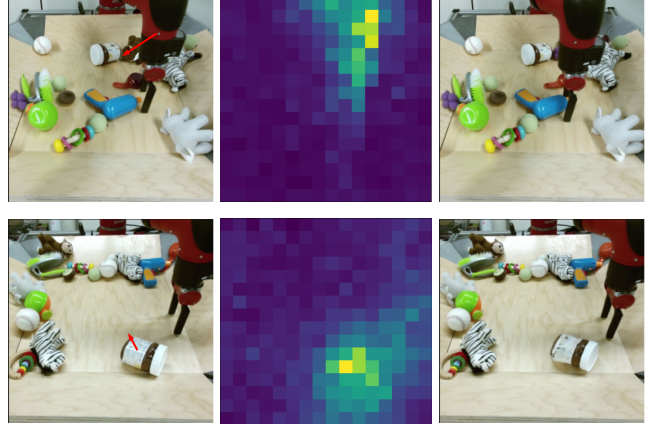


Figure 9: The attention maps from the last layer of the vector field regressor between the interacted location and the rest of the image, averaged over the heads and the flow integration path. It can be seen that the attention maps roughly cover the extents of the objects.

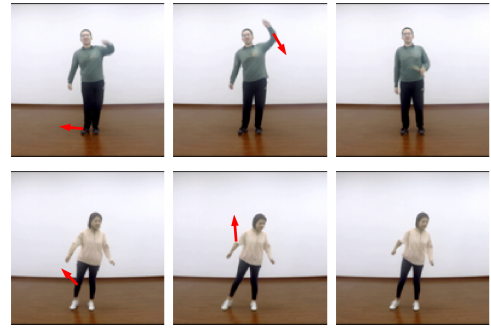


Figure 10: Examples of YODA simulating human motion on iPER. The images in the first column can be played as videos in Acrobat Reader.

location and the rest of the image (see middle column in Figure 9). These attention maps often correspond to coarse segmentations of the controlled objects. Finally, we provide some control sequences on the iPER dataset to show that YODA simulates realistic motions of humans (see Figure 10). More qualitative results, including possible applications of YODA, are in the supplementary materials.

## 5. Conclusion

In this paper we introduced YODA, a novel method for controllable video generation from sparse motion input. Our experimental evaluation demonstrates the ability of YODA to generate realistic multi-object videos, which involves learning the extents and interactions between multiple objects despite only passively observing their correlated motions.



**Acknowledgements** This work was supported by grant 188690 of the Swiss National Science Foundation.

## A. Architecture and training details

**Autoencoder.** We trained a VQGAN [15] autoencoder per dataset, using the official `taming transformers` repository.<sup>1</sup> The configurations of the VQGANs can be found in Table 4. Notice that we did not use a discriminator for the CLEVRER [68] dataset.

**Sparse optical flow encoder.** The  $16 \times 16$  tiled grid of sparse optical flow inputs is reshaped and linearly projected to 256 256-dimensional vectors that are fed into 5 subsequent blocks of (batch normalization [30], fully-connected layer and gelu activation [20]). The activation is omitted in the last block. This procedure results into a representation of the control input as 256 256-dimensional vectors.

**Training.** All models are trained for 300K iterations with the AdamW [41] optimizer with the base learning rate equal to  $10^{-4}$  and weight decay  $5 \cdot 10^{-6}$ . A learning rate linear warmup for 5K iterations is applied as well as a square root decay schedule. For the CLEVRER [68] dataset, following [11], random color jittering is additionally used to prevent overfitting. For the iPER [39] dataset, a random horizontal flip and a random time reversal is applied to prevent overfitting to the pose of the human. As suggested in [11], we used  $\sigma_{\min} = 10^{-7}$  in the flow matching loss [38] in all the experiments. In the final models, we used  $n_c = 5$  optical flow vectors for the control input.

## B. Qualitative results

In this section we provide more qualitative results with YODA. For videos, please, visit our project’s website <https://araachie.github.io/yoda>. Figures 11 and 12 contain some selected sequences to demonstrate the quality of separate frames, which is not visible in the videos on the webpage due to gif compression. Figure 11 contains more object manipulation scenarios on the BAIR [14] dataset. Figure 12 provides generated videos capturing long-range consequences of the input controls on the CLEVRER [68] dataset. Notice the ability of YODA to realistically model the physics of the scene. YODA was designed to make it possible to intervene into the generation process at any timestamp, which allows communicating new impulses to the objects on the fly.

## C. Demo

To ease the access to our results, we designed a demo of YODA. The user can load the pretrained models and directly interact with the scene by dragging objects with the mouse. The model responds by generating a subsequent

frame taking into account the controls specified by the user as well as the previously generated images (see the video on the website). The demo and the code will be released to the public.

## D. Applications

Pretrained YODA generates realistic responses to control. This opens up the opportunity to interact with the scene in a counterfactual way, which makes it possible to apply YODA to downstream tasks. In theory, by optimizing the control inputs to match the given video, one can solve planning or compress the video to a single frame and a sequence of controls. Here we discuss another possible application, object segmentation.

Given an image  $x$  of a scene with multiple objects and YODA trained on videos capturing that scene, the user selects a pixel on the object of interest. A random control is then applied to that location to generate the response  $x'$  with YODA. The optical flow field  $w$  between  $x$  and  $x'$  is calculated. All the vectors in  $w$  are compared with the input control using some similarity measure (can be  $l_2$  or cosine distance). We then apply a threshold to the result to obtain the segmentation mask. For robustness, this procedure can be repeated multiple times and the union of the resulting masks can be used as the final estimator of the segmentation mask. For an example, see Figure 13.

## References

- [1] Michael S Albergo and Eric Vanden-Eijnden. Building normalizing flows with stochastic interpolants. *arXiv preprint arXiv:2209.15571*, 2022. 2, 3
- [2] Mohammad Babaeizadeh, Chelsea Finn, D. Erhan, Roy H. Campbell, and Sergey Levine. Stochastic variational video prediction. *ArXiv*, abs/1710.11252, 2018. 2, 3
- [3] Mohammad Babaeizadeh, Mohammad Taghi Saffar, Suraj Nair, Sergey Levine, Chelsea Finn, and Dumitru Erhan. Fitvid: Overfitting in pixel-level video prediction. *arXiv preprint arXiv:2106.13195*, 2021. 2, 3
- [4] Fan Bao, Chongxuan Li, Yue Cao, and Jun Zhu. All are worth words: a vit backbone for score-based diffusion models. *arXiv preprint arXiv:2209.12152*, 2022. 4
- [5] Andreas Blattmann, Timo Milbich, Michael Dorkenwald, and Björn Ommer. ipoke: Poking a still image for controlled stochastic video synthesis. In *Proceedings of the IEEE/CVF International Conference on Computer Vision*, pages 14707–14717, 2021. 2, 4, 5, 6, 7
- [6] Andreas Blattmann, Timo Milbich, Michael Dorkenwald, and Björn Ommer. Understanding object dynamics for interactive image-to-video synthesis. In *Proceedings of the IEEE/CVF Conference on Computer Vision and Pattern Recognition*, pages 5171–5181, 2021. 2, 7
- [7] Ricky TQ Chen, Yulia Rubanova, Jesse Bettencourt, and David K Duvenaud. Neural ordinary differential equations. *Advances in neural information processing systems*, 31, 2018. 3

<sup>1</sup><https://github.com/CompVis/taming-transformers>

	CLEVRER 128 × 128 [68]	BAIR 256 × 256 [14]	iPER 128 × 128 [39]
embed_dim	4	8	4
n_embed	8192	16384	16384
double_z	False	False	False
z_channels	4	8	4
resolution	128	256	128
in_channels	3	3	3
out_ch	3	3	3
ch	128	128	128
ch_mult	[1,2,2,4]	[1,1,2,2,4]	[1,2,2,4]
num_res_blocks	2	2	2
attn_resolutions	[16]	[16]	[32]
dropout	0.0	0.0	0.0
disc_conditional	-	False	False
disc_in_channels	-	3	3
disc_start	-	20k	20k
disc_weight	-	0.8	0.8
codebook_weight	-	1.0	1.0

Table 4: Configurations of VQGAN [15] for different datasets.



Figure 11: Different scene manipulations with YODA on the BAIR [14] dataset. Please, use Acrobat Reader to play the frames in the leftmost column or visit our project’s website <https://araachie.github.io/yoda>.

- [8] Silvia Chiappa, Sébastien Racaniere, Daan Wierstra, and Shakir Mohamed. Recurrent environment simulators. *arXiv preprint arXiv:1704.02254*, 2017. 2
- [9] Aidan Clark, Jeff Donahue, and Karen Simonyan. Adversarial video generation on complex datasets. *arXiv: Computer Vision and Pattern Recognition*, 2019. 2
- [10] Aram Davtyan and Paolo Favaro. Controllable video generation through global and local motion dynamics. In Shai Avidan, Gabriel Brostow, Moustapha Cissé, Giovanni Maria Farinella, and Tal Hassner, editors, *Computer Vision – ECCV 2022*, pages 68–84, Cham, 2022. Springer Nature Switzerland. 2, 7
- [11] Aram Davtyan, Sepehr Sameni, and Paolo Favaro. Randomized conditional flow matching for video prediction. *arxiv*, 2022. 2, 3, 9
- [12] Emily Denton and Rob Fergus. Stochastic video generation with a learned prior. In *International conference on machine learning*, pages 1174–1183. PMLR, 2018. 2, 3
- [13] Prafulla Dhariwal and Alex Nichol. Diffusion models beat gans on image synthesis. *ArXiv*, abs/2105.05233, 2021. 2
- [14] Frederik Ebert, Chelsea Finn, Alex X. Lee, and Sergey Levine. Self-supervised visual planning with temporal skip connections. In *CoRL*, 2017. 6, 9, 10
- [15] Patrick Esser, Robin Rombach, and Bjorn Ommer. Taming transformers for high-resolution image synthesis. In *Proceedings of the IEEE/CVF conference on computer vision and pattern recognition*, pages 12873–12883, 2021. 2, 3, 9, 10
- [16] Chelsea Finn, Ian Goodfellow, and Sergey Levine. Unsupervised learning for physical interaction through video prediction. *Advances in neural information processing systems*, 29, 2016. 2

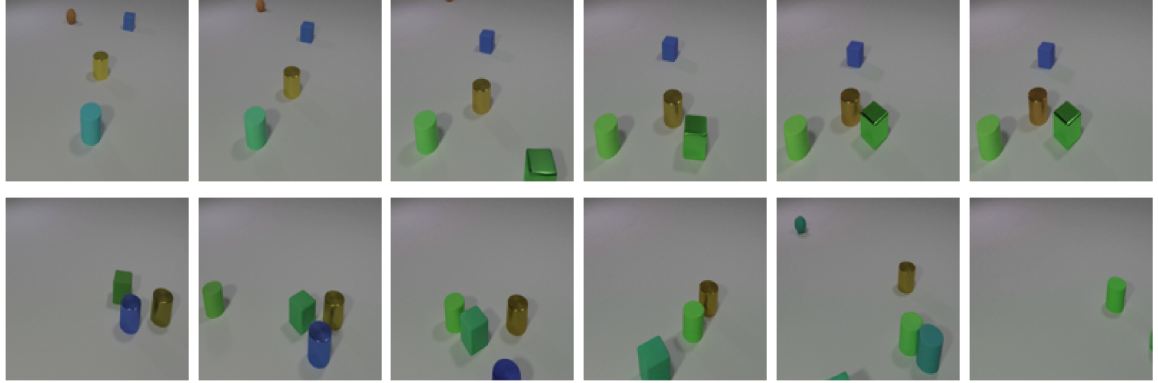


Figure 12: Videos generated with YODA on the CLEVRER [68] dataset. Please, use Acrobat Reader to play the frames in the leftmost column or visit our project’s website <https://araachie.github.io/yoda>.

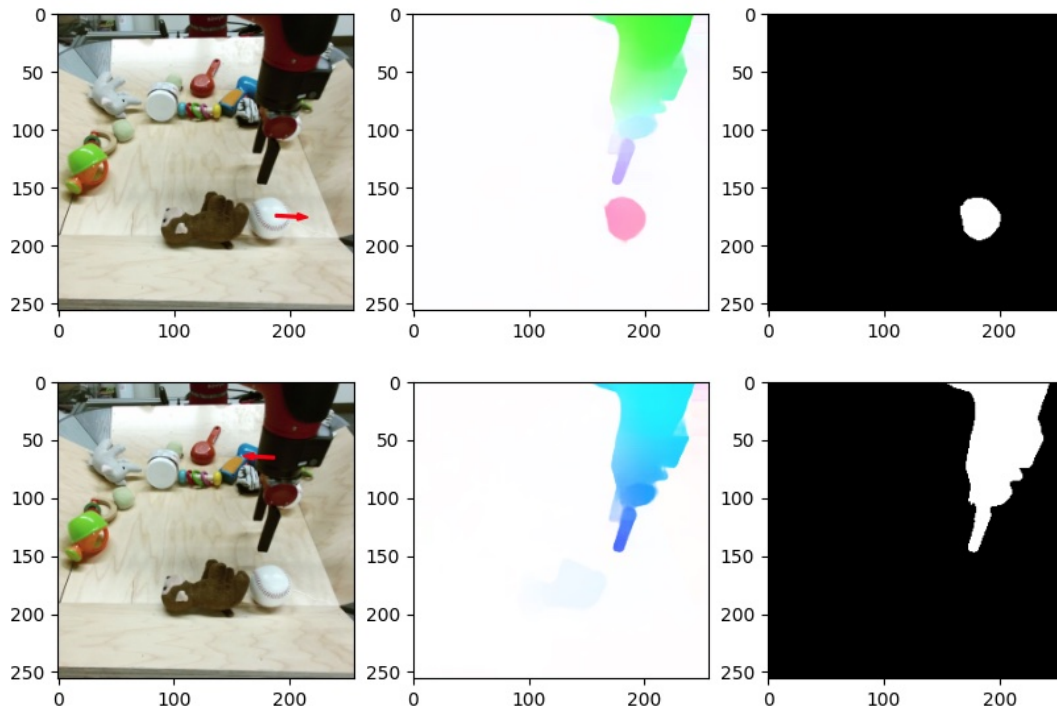


Figure 13: From left to right: the input image, the optical flow between the input image and the next one, the estimated mask. The red arrows in the images in the first column show the control input.

- [17] Agrim Gupta, Stephen Tian, Yunzhi Zhang, Jiajun Wu, Roberto Martín-Martín, and Li Fei-Fei. Maskvit: Masked visual pre-training for video prediction. *arXiv preprint arXiv:2206.11894*, 2022. 2, 3
- [18] Zekun Hao, Xun Huang, and Serge Belongie. Controllable video generation with sparse trajectories. In *Proceedings of the IEEE Conference on Computer Vision and Pattern Recognition*, pages 7854–7863, 2018. 2, 7
- [19] William Harvey, Saeid Naderiparizi, Vaden Masrani, Christian Weilbach, and Frank Wood. Flexible diffusion modeling of long videos. *arXiv preprint arXiv:2205.11495*, 2022. 2
- [20] Dan Hendrycks and Kevin Gimpel. Gaussian error linear units (gelus). *arXiv preprint arXiv:1606.08415*, 2016. 9
- [21] Jonathan Ho, William Chan, Chitwan Saharia, Jay Whang, Ruiqi Gao, Alexey Gritsenko, Diederik P Kingma, Ben Poole, Mohammad Norouzi, David J Fleet, et al. Imagen video: High definition video generation with diffusion models. *arXiv preprint arXiv:2210.02303*, 2022. 2
- [22] Jonathan Ho, Ajay Jain, and P. Abbeel. Denoising diffusion probabilistic models. *ArXiv*, abs/2006.11239, 2020. 3



- [23] Jonathan Ho and Tim Salimans. Classifier-free diffusion guidance. *arXiv preprint arXiv:2207.12598*, 2022. 4
- [24] Jonathan Ho, Tim Salimans, Alexey Gritsenko, William Chan, Mohammad Norouzi, and David J Fleet. Video diffusion models. *arXiv preprint arXiv:2204.03458*, 2022. 2
- [25] Sepp Hochreiter and Jürgen Schmidhuber. Long short-term memory. *Neural Comput.*, 9(8):1735–1780, nov 1997. 3
- [26] Tobias Höppe, Arash Mehrjou, Stefan Bauer, Didrik Nielsen, and Andrea Dittadi. Diffusion models for video prediction and infilling. *arXiv preprint arXiv:2206.07696*, 2022. 2
- [27] Qiyang Hu, Adrian Wälchli, Tiziano Portenier, Matthias Zwicker, and Paolo Favaro. Learning to take directions one step at a time. In *2020 25th International Conference on Pattern Recognition (ICPR)*, pages 739–746. IEEE, 2021. 2
- [28] Yaosi Hu, Chong Luo, and Zhenzhong Chen. Make it move: Controllable image-to-video generation with text descriptions. In *Proceedings of the IEEE/CVF Conference on Computer Vision and Pattern Recognition*, pages 18219–18228, 2022. 3
- [29] Jiahui Huang, Yuhe Jin, Kwang Moo Yi, and Leonid Sigal. Layered controllable video generation. In Shai Avidan, Gabriel Brostow, Moustapha Cissé, Giovanni Maria Farinella, and Tal Hassner, editors, *Computer Vision – ECCV 2022*, pages 546–564, Cham, 2022. Springer Nature Switzerland. 2, 7
- [30] Sergey Ioffe and Christian Szegedy. Batch normalization: Accelerating deep network training by reducing internal covariate shift. In *International conference on machine learning*, pages 448–456. pmlr, 2015. 9
- [31] Michael Janner, Sergey Levine, William T Freeman, Joshua B Tenenbaum, Chelsea Finn, and Jiajun Wu. Reasoning about physical interactions with object-oriented prediction and planning. *arXiv preprint arXiv:1812.10972*, 2018. 3
- [32] Tero Karras, Miika Aittala, Samuli Laine, Erik Härkönen, Janne Hellsten, Jaakko Lehtinen, and Timo Aila. Alias-free generative adversarial networks. *Advances in Neural Information Processing Systems*, 34:852–863, 2021. 2
- [33] Seung Wook Kim, Yuhao Zhou, Jonah Philion, Antonio Torralba, and Sanja Fidler. Learning to simulate dynamic environments with gamegan. In *Proceedings of the IEEE/CVF Conference on Computer Vision and Pattern Recognition*, pages 1231–1240, 2020. 2
- [34] Yunji Kim, Seonghyeon Nam, In Cho, and Seon Joo Kim. Unsupervised keypoint learning for guiding class-conditional video prediction. *Advances in neural information processing systems*, 32, 2019. 2
- [35] Guillaume Le Moing, Jean Ponce, and Cordelia Schmid. Ccvs: Context-aware controllable video synthesis. *Advances in Neural Information Processing Systems*, 34:14042–14055, 2021. 2, 3
- [36] Alex X Lee, Richard Zhang, Frederik Ebert, Pieter Abbeel, Chelsea Finn, and Sergey Levine. Stochastic adversarial video prediction. *arXiv preprint arXiv:1804.01523*, 2018. 2, 3, 7
- [37] Wonkwang Lee, Whie Jung, Han Zhang, Ting Chen, Jing Yu Koh, Thomas E. Huang, Hyungsuk Yoon, Honglak Lee, and Seunghoon Hong. Revisiting hierarchical approach for persistent long-term video prediction. *ArXiv*, abs/2104.06697, 2021. 2
- [38] Yaron Lipman, Ricky TQ Chen, Heli Ben-Hamu, Maximilian Nickel, and Matt Le. Flow matching for generative modeling. *arXiv preprint arXiv:2210.02747*, 2022. 2, 3, 9
- [39] Wen Liu, Zhixin Piao, Jie Min, Wenhan Luo, Lin Ma, and Shenghua Gao. Liquid warping gan: A unified framework for human motion imitation, appearance transfer and novel view synthesis. In *Proceedings of the IEEE/CVF International Conference on Computer Vision*, pages 5904–5913, 2019. 6, 9, 10
- [40] Xingchao Liu, Chengyue Gong, and Qiang Liu. Flow straight and fast: Learning to generate and transfer data with rectified flow. *arXiv preprint arXiv:2209.03003*, 2022. 2, 3
- [41] Ilya Loshchilov and Frank Hutter. Decoupled weight decay regularization. In *ICLR*, 2019. 9
- [42] Pauline Luc, Aidan Clark, Sander Dieleman, Diego de Las Casas, Yotam Doron, Albin Cassirer, and Karen Simonyan. Transformation-based adversarial video prediction on large-scale data. *ArXiv*, abs/2003.04035, 2020. 2
- [43] Willi Menapace, Stéphane Lathuilière, Aliaksandr Siarohin, Christian Theobalt, Sergey Tulyakov, Vladislav Golyanik, and Elisa Ricci. Playable environments: Video manipulation in space and time. In *Proceedings of the IEEE/CVF Conference on Computer Vision and Pattern Recognition*, pages 3584–3593, 2022. 2, 3
- [44] Willi Menapace, Stéphane Lathuilière, Sergey Tulyakov, Aliaksandr Siarohin, and Elisa Ricci. Playable video generation. In *Proceedings of the IEEE/CVF Conference on Computer Vision and Pattern Recognition*, pages 10061–10070, 2021. 2, 7
- [45] Manuel Serra Nunes, Atabak Dehban, Plinio Moreno, and José Santos-Victor. Action-conditioned benchmarking of robotic video prediction models: a comparative study. In *2020 IEEE International Conference on Robotics and Automation (ICRA)*, pages 8316–8322. IEEE, 2020. 2
- [46] Junhyuk Oh, Xiaoxiao Guo, Honglak Lee, Richard L Lewis, and Satinder Singh. Action-conditional video prediction using deep networks in atari games. *Advances in neural information processing systems*, 28, 2015. 2
- [47] Gaurav Parmar, Richard Zhang, and Junyan Zhu. On aliased resizing and surprising subtleties in gan evaluation. *2022 IEEE/CVF Conference on Computer Vision and Pattern Recognition (CVPR)*, pages 11400–11410, 2022. 5
- [48] Judea Pearl and Dana Mackenzie. *The book of why: the new science of cause and effect*. Basic books, 2018. 1
- [49] Ruslan Rakhimov, Denis Volkhonskiy, Alexey Artemov, Denis Zorin, and Evgeny Burnaev. Latent video transformer. *arXiv preprint arXiv:2006.10704*, 2020. 2, 3
- [50] Robin Rombach, Andreas Blattmann, Dominik Lorenz, Patrick Esser, and Björn Ommer. High-resolution image synthesis with latent diffusion models. In *Proceedings of the IEEE/CVF Conference on Computer Vision and Pattern Recognition*, pages 10684–10695, 2022. 2
- [51] Oleh Rybkin, Karl Pertsch, Konstantinos G Derpanis, Kostas Daniilidis, and Andrew Jaegle. Learning what you can do be-

- fore doing anything. *arXiv preprint arXiv:1806.09655*, 2018. 2
- [52] Karl Schmeckpeper, Georgios Georgakis, and Kostas Daniilidis. Object-centric video prediction without annotation. In *2021 IEEE International Conference on Robotics and Automation (ICRA)*, pages 13604–13610. IEEE, 2021. 3
- [53] Younggyo Seo, Kimin Lee, Fangchen Liu, Stephen James, and P. Abbeel. Harp: Autoregressive latent video prediction with high-fidelity image generator. *ArXiv*, abs/2209.07143, 2022. 2, 3
- [54] Uriel Singer, Adam Polyak, Thomas Hayes, Xi Yin, Jie An, Songyang Zhang, Qiyuan Hu, Harry Yang, Oron Ashual, Oran Gafni, et al. Make-a-video: Text-to-video generation without text-video data. *arXiv preprint arXiv:2209.14792*, 2022. 2
- [55] Zachary Teed and Jia Deng. Raft: Recurrent all-pairs field transforms for optical flow. In *Computer Vision–ECCV 2020: 16th European Conference, Glasgow, UK, August 23–28, 2020, Proceedings, Part II 16*, pages 402–419. Springer, 2020. 5, 7
- [56] Sergey Tulyakov, Ming-Yu Liu, Xiaodong Yang, and Jan Kautz. Mocogan: Decomposing motion and content for video generation. In *Proceedings of the IEEE conference on computer vision and pattern recognition*, pages 1526–1535, 2018. 7
- [57] Thomas Unterthiner, Sjoerd van Steenkiste, Karol Kurach, Raphaël Marinier, Marcin Michalski, and Sylvain Gelly. Towards accurate generative models of video: A new metric & challenges. *ArXiv*, abs/1812.01717, 2018. 5
- [58] Ashish Vaswani, Noam Shazeer, Niki Parmar, Jakob Uszkoreit, Llion Jones, Aidan N Gomez, Łukasz Kaiser, and Illia Polosukhin. Attention is all you need. In I. Guyon, U. Von Luxburg, S. Bengio, H. Wallach, R. Fergus, S. Vishwanathan, and R. Garnett, editors, *Advances in Neural Information Processing Systems*, volume 30. Curran Associates, Inc., 2017. 3, 8
- [59] Vikram Voleti, Alexia Jolicoeur-Martineau, and Christopher Pal. Mcvd: Masked conditional video diffusion for prediction, generation, and interpolation. *arXiv preprint arXiv:2205.09853*, 2022. 2
- [60] Yaohui Wang, Piotr Bilinski, Francois Bremond, and Antitza Dantcheva. Imaginator: Conditional spatio-temporal gan for video generation. In *Proceedings of the IEEE/CVF Winter Conference on Applications of Computer Vision*, pages 1160–1169, 2020. 2
- [61] Zhou Wang, Alan Conrad Bovik, Hamid R. Sheikh, and Eero P. Simoncelli. Image quality assessment: from error visibility to structural similarity. *IEEE Transactions on Image Processing*, 13:600–612, 2004. 5
- [62] Dirk Weissenborn, Oscar Täckström, and Jakob Uszkoreit. Scaling autoregressive video models. *arXiv preprint arXiv:1906.02634*, 2019. 3
- [63] Nevan Wichers, Ruben Villegas, D. Erhan, and Honglak Lee. Hierarchical long-term video prediction without supervision. *ArXiv*, abs/1806.04768, 2018. 2
- [64] Yi-Fu Wu, Jaesik Yoon, and Sungjin Ahn. Generative video transformer: Can objects be the words? In *International Conference on Machine Learning*, pages 11307–11318. PMLR, 2021. 3
- [65] Wilson Yan, Ryo Okumura, Stephen James, and Pieter Abbeel. Patch-based object-centric transformers for efficient video generation. *arXiv preprint arXiv:2206.04003*, 2022. 3
- [66] Wilson Yan, Yunzhi Zhang, Pieter Abbeel, and Aravind Srinivas. Videogpt: Video generation using vq-vae and transformers. *arXiv preprint arXiv:2104.10157*, 2021. 2
- [67] Ruihan Yang, Prakhar Srivastava, and Stephan Mandt. Diffusion probabilistic modeling for video generation. *arXiv preprint arXiv:2203.09481*, 2022. 2
- [68] Kexin Yi, Chuang Gan, Yunzhu Li, Pushmeet Kohli, Jiajun Wu, Antonio Torralba, and Joshua B. Tenenbaum. Clevrer: Collision events for video representation and reasoning. *ArXiv*, abs/1910.01442, 2020. 6, 9, 10, 11
- [69] Jiji Zhang and Peter Spirtes. Intervention, determinism, and the causal minimality condition. *Synthese*, 182:335–347, 2011. 1
- [70] Richard Zhang, Phillip Isola, Alexei A Efros, Eli Shechtman, and Oliver Wang. The unreasonable effectiveness of deep features as a perceptual metric. In *Proceedings of the IEEE conference on computer vision and pattern recognition*, pages 586–595, 2018. 5